High-efficiency solution processable polymer photovoltaic cells by self-organization of polymer blends

GANG LI[1], VISHAL SHROTRIYA[1], JINSONG HUANG[1], YAN YAO[1], TOM MORIARTY[2], KEITH EMERY[2] AND YANG YANG[1]*

[1]Department of Materials Science and Engineering, University of California Los Angeles, Los Angeles, California 90095, USA
[2]National Renewable Energy Laboratory, Golden, Colorado 80401, USA
*e-mail: yangy@ucla.edu

Published online: 9 October 2005; doi:10.1038/nmat1500

Converting solar energy into electricity provides a much-needed solution to the energy crisis the world is facing today. Polymer solar cells have shown potential to harness solar energy in a cost-effective way. Significant efforts are underway to improve their efficiency to the level of practical applications. Here, we report highly efficient polymer solar cells based on a bulk heterojunction of polymer poly(3-hexylthiophene) and methanofullerene. Controlling the active layer growth rate results in an increased hole mobility and balanced charge transport. Together with increased absorption in the active layer, this results in much-improved device performance, particularly in external quantum efficiency. The power-conversion efficiency of 4.4% achieved here is the highest published so far for polymer-based solar cells. The solution process involved ensures that the fabrication cost remains low and the processing is simple. The high efficiency achieved in this work brings these devices one step closer to commercialization.

Polymer solar cells have evolved as a promising cost-effective alternative to silicon-based solar cells[1–3]. Some of the important advantages of these so-called 'plastic' solar cells include low cost of fabrication, ease of processing, mechanical flexibility and versatility of chemical structure from advances in organic chemistry. However, low efficiency[4–6] of these plastic solar cells limits their feasibility for commercial use. The efficiencies of polymer photovoltaic (PV) cells got a major boost with the introduction of the bulk heterojunction (BHJ) concept[7,8] consisting of an interpenetrating network of electron donor and acceptor materials. This concept has also been demonstrated in small-molecular organic PVs[9]. It is argued that owing to the space–charge effects inherent in the BHJ structure, the fill factor (FF) is usually low and the disordered structure will be ultimately limited by high series resistance[10]. To achieve a highly efficient PV device, solar radiation needs to be efficiently absorbed, for which the device thickness needs to be increased. However, this will further increase the series resistance of the device. Here we demonstrate that the series resistance of the polymer BHJ PV cells can be significantly reduced by polymer self-organization (to values as low as 1.56 Ω cm^2) by controlling the growth rate of the active polymer layer from solution to solid state. The FF also increased to a value of more than 67%, which is among the highest values reported for polymer solar cells. As a result, we achieved device power conversion efficiency (PCE) of 4.4% under the standard AM1.5G 1 Sun test condition. The PV cells fabricated in this study are made by a solution-based process and large device area can be achieved by this process at relatively low cost.

The polymer PV device in this study consisted of an active layer of poly(3-hexylthiophene): [6,6]-phenyl-C_{61}-butyric acid methyl ester (P3HT/PCBM) sandwiched between metallic electrodes. The thickness of the active layer was ~210–230 nm and the active device area was roughly 0.11 cm^2. The growth rate of the polymer layer was controlled by varying the film solidification time. The details on device fabrication process and characterization

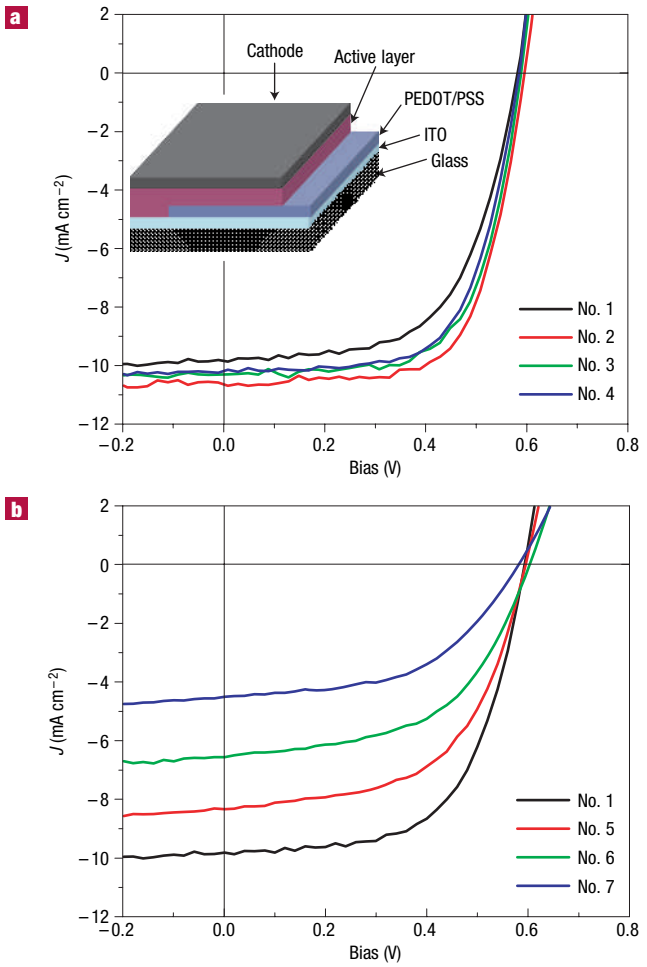

Figure 1 Effect of thermal annealing and film growth rate on the performance of the plastic solar cells. a, The different *J–V* curves correspond to the devices with active layer before (no. 1) and after thermal annealing at 110 °C for 10 min (no. 2), 20 min (no. 3) and 30 min (no. 4). The active layer thickness was ~210 nm and the film growth time was ~20 min. **b**, *J–V* characteristics under illumination for devices with different film growth rates by varying the solvent evaporation time, t_{evp}. The t_{evp} for different films were 20 min (no. 1), 3 min (no. 5), 40 s (no. 6) and 20 s (no. 7).

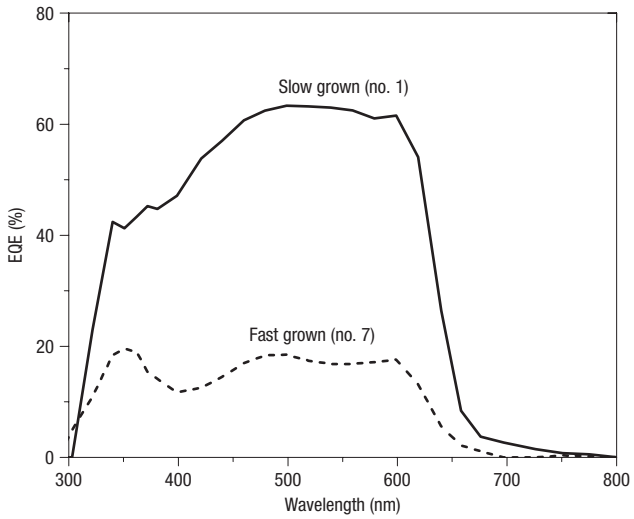

Figure 2 Effect of film growth rate on EQE of polymer solar cells. EQE measurements are plotted for P3HT/PCBM photovoltaic cells for two types of active layer: slow grown (no. 1) and fast grown (no. 7). The efficiency maximum for slow-grown film is ~63% which is more than three times that of fast-grown film (~19%).

techniques are given in the Methods section. Encapsulated devices were brought to the National Renewable Energy Laboratory (NREL), Colorado, for testing under the Standard Test Condition (STC). On the basis of the mismatch between the efficiency measurements at University of California Los Angeles (UCLA) and NREL, a correction factor was created by the UCLA team and applied to similar measurements done at UCLA (see Methods for details). The current–voltage (*J–V*) curves under illumination for four devices with annealing times (t_A) of 0 (device no. 1), 10 (no. 2), 20 (no. 3) and 30 min (no. 4) are shown in Fig. 1a. The annealing was performed at 110 °C. After annealing for 10 minutes (device no. 2), the short-circuit current (J_{SC}) increases slightly from 9.9 to 10.6 mA cm^{-2} and the FF increases from 60.3 to 67.4%, which is among the highest FFs in organic solar cells. The open-circuit voltage (V_{OC}) remains unchanged after annealing. As a result, the PCE improves from 3.5% (no. 1) to 4.4% (no. 2). Under the dark conditions, the rectification ratios are close to 10^7 at a bias of 2 V for all four devices. The reason behind the high FFs of our devices is believed to be the significantly large thickness of the active layer. The thickness of the active layer makes it free of pinholes and microcracks and all devices show very high shunt resistance of 180–640 MΩ as derived from the *J–V* characteristics measured under dark conditions. To our knowledge, these values are the highest reported for organic solar cells. The ultrahigh shunt resistance reduces the noise equivalent power (NEP) of the device and makes it ideal for photodetector applications. Moreover, the surface of the active layer becomes smoother on annealing, which enables a very good, defect-free contact with the metal cathode, thereby increasing the FF values. Based on 16 devices of the same kind (no. 2, $t_A = 10$ min), the efficiency variation is $4.2 \pm 0.2\%$. Although the formerly highest reported PV cell efficiency is for a P3HT/PCBM system in the 1:2 wt/wt ratio[5], various independent studies have shown that the 1:1 wt/wt ratio should be superior[11,12]. It has also been reported that to absorb greater than 95% of the incident light over the wavelength range of 450–600 nm, a P3HT film of 240 nm thickness is needed[2]. With P3HT/PCBM of 1:1 wt/wt ratio and the reflective cathode, 210–230-nm-thick P3HT/PCBM film efficiently absorbs incident light. It is widely believed that the fundamental limitation of the photocurrent of polymer solar cells is because of the low mobility of the holes in donor polymer[3]. Compared with the devices with P3HT/PCBM of 1:2 wt/wt ratio, the donor/acceptor network transports holes more efficiently in 1:1 wt/wt ratio, resulting in a more balanced electron and hole transport. Time-of-flight (TOF) measurements on P3HT/PCBM blend films with different wt/wt ratios verified that only 1:1 wt/wt ratio film gives balanced, non-dispersive electron and hole transport. The much improved FF of 67.4% for our devices supports this argument.

The highly regular chain structure of poly(3-alkylthiophene)s (P3ATs) facilitates their self-organization into two-dimensional sheets by means of inter-chain stacking[13]. Self-organization has been shown to improve field-effect carrier mobility in RR-P3HT by more than a factor of 100 to 0.1 cm^2 V^{-1} s^{-1} (refs 14,15). The slow growth will assist the formation of self-organized ordered structure in the P3HT/PCBM blend system. However, the ordering in this blend system might be different from the kind of ordering

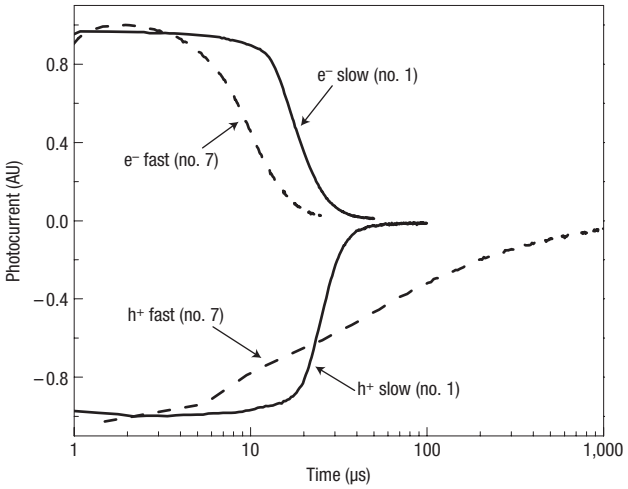

Figure 3 Effect of film growth rate on the mobility of charge carriers in the active layer. TOF signals of slow-grown (no. 1) and fast-grown (no. 7) films plotted in a semi-log scale. Note that μ_h in fast-grown film (no. 7) is significantly lower compared with μ_e in the film, as well as compared with μ_h and μ_e in the slow-grown film (no. 1). Also, the hole transport is dispersive in film no. 7 and the carrier transport is unbalanced. Films in TOF devices were prepared the same way as cells in this study and their film thickness is ~1 μm.

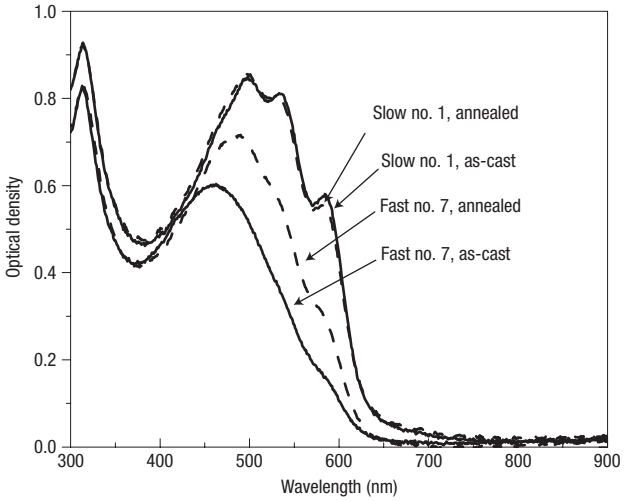

Figure 4 Effect of film growth rate and thermal annealing on the absorbance of the P3HT/PCBM films. Ultraviolet–visible absorption spectra for films of P3HT/PCBM (in 1:1 wt/wt ratio), for both slow-grown (no. 1) and fast-grown (no. 7) films, before (solid line) and after (dashed line) annealing. The films were spun cast at 600 r.p.m. for 60 s (film thickness ~ 210 nm) and the annealing was done at 110 °C for 20 min.

observed for pristine P3HT films, in the sense that the presence of PCBM molecules will have an effect on the stacking of the polymer chains[16]. The degree of self-organization can be varied by controlling the film growth rate or, in other words, by controlling the time it takes for the wet films to solidify. In Fig. 1b we compare the *J–V* characteristics of four devices with different solvent evaporation times (t_{evp}) after spin-coating, judging by visual inspection of the change in film colour when it solidifies from the liquid phase. Device no. 1 was covered in a glass petri dish while drying and had $t_{evp} \sim 20$ min, no. 5 was left open in N_2 ambient and had $t_{evp} \sim 3$ min, no. 6 and no. 7 were dried by putting on hot plate at 50 and 70 °C, respectively, and had $t_{evp} \sim 40$ and 20 s. The J_{SC} reduces from 9.9 to 8.3, 6.6 and 4.5 mA cm^{-2}, and the device series resistance, R_{SA}, increases from 2.4 to 4.5, 12.5 and 19.8 Ω cm^2 with reducing t_{evp}. Series and shunt resistances were derived from the slope of the *J–V* characteristic curve under dark conditions close to 2 and 0 V, respectively[17]. The FF also consistently decreases from 60.3 to 52.0%. The low R_{SA} of 2.4 Ω cm^2 (for device no. 1) achieved is comparable to that of much thinner devices[18] (~48 nm), underlining the effect of self-organization. The summary of device performance for various PV devices fabricated in this work (device nos 1–7) is provided in Table 1. Figure 2 shows the results of external quantum efficiency (EQE) measurements for two types of device, slow grown (no. 1) and fast grown (no. 7). The parameters for the highest efficiency device (no. 2) are shown in bold. The EQE for the device with fast-grown film shows a maximum of ~19% at a wavelength of 350 nm. On the other hand, for the device with slow-grown film, the EQE maximum increases by more than a factor of three to ~63% at 500 nm. The integral of the product of this absolute EQE and the global reference spectrum yields a J_{SC} of 9.47 mA cm^{-2}, which matches closely to the J_{SC} that we measured for this particular device. This increase in EQE over the wavelength range of 350–650 nm contributes to the increase in the PCE of our devices. We believe that this enhancement in EQE originates from two important contributions, an increase in the charge-carrier mobility and increased absorption in the active layer. The discussion on the effect of slow growth rate on the charge-carrier mobility and the absorption spectra of the films follows.

Table 1 Summary of device performance for various PV devices in the work.

Device no.	J_{SC} (mA cm^{-2})	V_{OC} (V)	PCE (%)	FF (%)	R_{SA} (Ω cm^2)
1	9.86	0.59	3.52	60.3	2.4
2	**10.6**	**0.61**	**4.37**	**67.4**	**1.7**
3	10.3	0.60	4.05	65.5	1.6
4	10.3	0.60	3.98	64.7	1.6
5	8.33	0.60	2.80	56.5	4.9
6	6.56	0.60	2.10	53.2	12.5
7	4.50	0.58	1.36	52.0	19.8

A TOF study was conducted on slow-grown (no. 1) and fast-grown (no. 7) films at an electric field strength of $E \sim 2 \times 10^5$ V cm^{-1}. The film-preparation method for TOF measurements was the same as that for device fabrication to maintain maximum similarity for reliable comparison. As clearly seen in Fig. 3, in the film prepared with conditions similar to device no. 1 (or the slow-grown film), both the electrons and holes transport non-dispersively with electron and hole mobilities of $\mu_e = 7.7 \times 10^{-5}$ and $\mu_h = 5.1 \times 10^{-5}$ cm^2 V^{-1} s^{-1}, whereas for film no. 7, fast growth leads to dispersive hole transport and a significant reduction in μ_h to 5.1×10^{-6} cm^2 V^{-1} s^{-1}. The electron mobility increases slightly to 1.1×10^{-4} cm^2 V^{-1} s^{-1}. The destruction of ordered structure during fast growth is believed to be the reason for this. For the slow-grown film, μ_h is similar to (or slightly higher than) the values reported earlier for poly(*p*-phenylenevinylene)/PCBM blends[19,20] and the ratio between electron and hole mobilities is close to unity ($\mu_e/\mu_h \sim 1.5$) resulting in balanced carrier transport in the active layer. When the charge transport in the device is unbalanced (for example, in the pristine P3HT/PCBM system where μ_h is significantly lower than μ_e) hole accumulation occurs in the device and the

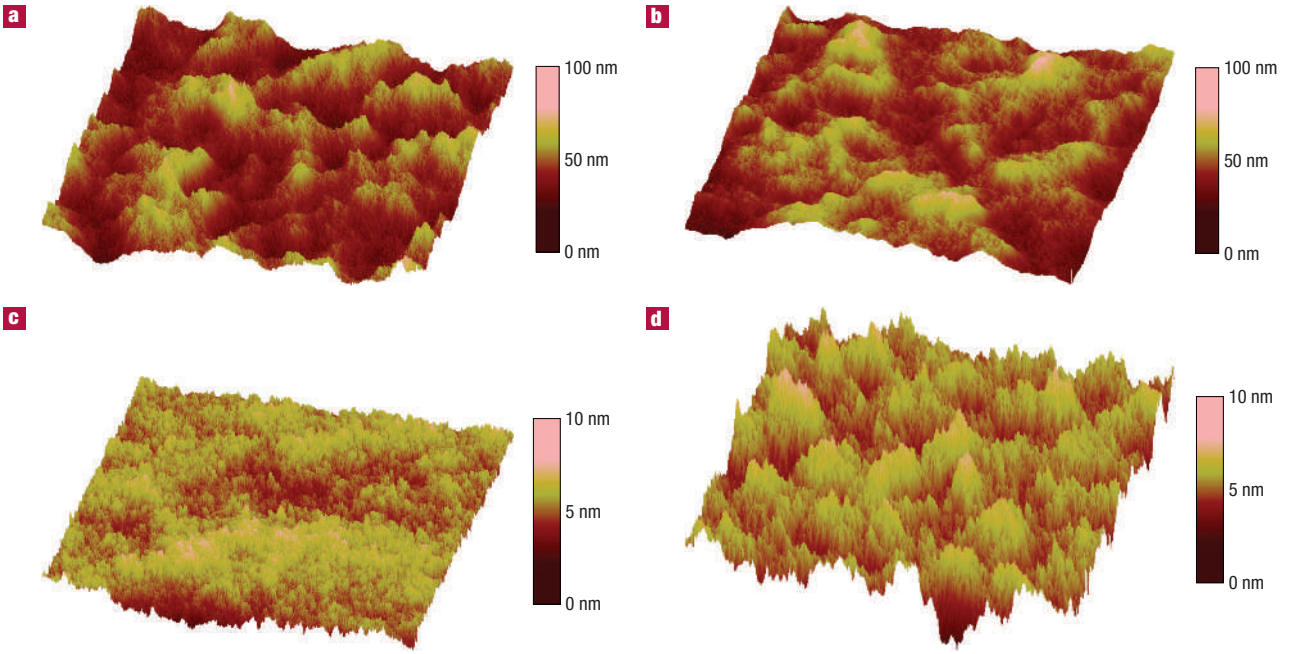

Figure 5 Effect of growth rate and thermal annealing on the morphology of the active layer. AFM height images of the P3HT/PCBM composite films (PCBM concentration = 50 wt%) showing a 5 μm × 5 μm surface area. **a**, Slow-grown film (no. 1) before thermal annealing. **b**, Slow-grown film (no. 1) after thermal annealing at 110 °C for 10 min. **c**, Fast-grown film (no. 7) before thermal annealing. **d**, Fast-grown film (no. 7) after thermal annealing at 110 °C for 20 min. Note that the colour scale for the films **a** and **b** is 0–100 nm, whereas for films **c** and **d** it is 0–10 nm.

photocurrent is space–charge limited[16]. The photocurrent is then governed by a square-root dependence on bias and an FF above 40% is unachievable[21]. However, when the carrier transport is more balanced, the current is not limited by space–charge effects and high FFs are possible. For example, blending PCBM into a poly(phenylene vinylene) derivative has shown to increase the hole mobility by a factor of 200 compared with the pristine polymer films, resulting in μ_h being lower than μ_e by only an order of magnitude[16]. As a result, FF values of up to 60% can be achieved for PV devices based on these polymer/PCBM blends[4]. For our devices μ_e/μ_h of only 1.5 results in FF values of more than 67%. For devices with active layer thickness larger than the mean carrier drift length of the charge carrier, the device performance is limited by the carrier with lower mean free path (holes)[22]. To maintain the electrical neutrality in the device, the unbalanced transport will result in a loss in efficiency by increased recombination. The more balanced transport of holes and electrons in slow-grown films will therefore result in better device performance. On the other hand, for the fast-grown film, the unbalanced electron and hole transport and the significantly reduced μ_h results in low photocurrent and poor FF.

The measured optical densities for slow-grown (no. 1) and fast-grown (no. 7) films are shown in Fig. 4, before and after thermal annealing at 110 °C for 20 min. Compared with the film dried at 70 °C (no. 7), the absorption in the red region of the slow grown film (no. 1) is much stronger. The three vibronic absorption shoulders (peaks) are much more pronounced in film no. 1, indicating a higher degree of ordering[23]. After annealing at 110 °C for 20 min, the absorbance of film no. 7 shows significant increase and the vibronic features become clearer, indicating a partial recovery of ordering. During the fast growth of the film, the orientation of P3HT supermolecules is forced by the short timescale and is not thermodynamically stable. On thermal annealing, the chains become mobile and self-organization can occur to form ordering. Significant red-shift appears in the more ordered films as high crystalline order involves an enhanced conjugation length and hence a shift of the absorption spectrum to lower energies[23]. The observed enhancement of conjugation length is consistent with our TOF results. As the film thickness is same for all four films, the change in absorption spectra is believed to be a result of increased inter-chain interaction and not because of an increase in film thickness. For the slow-grown film (no. 1), the absorption spectrum shows no significant difference before and after thermal annealing, further strengthening our argument that the slow-grown film already has a high degree of ordering. X-ray diffraction (XRD; Bede Microsource D1 Diffractometer) is a standard method for investigating crystalline structures. XRD studies on pure poly(3-alkylthiophene) films have been reported[13,24–26]. From the preliminary XRD measurements on the slow-grown P3HT/PCBM-blend films we could not clearly identify crystalline peaks. Although P3HT is among the polymers with highest degree of crystalline structure, P3HT film is still mostly amorphous. In the blend film, with 1:1 wt/wt ratio, P3HT and PCBM each act as heavily doped impurities of their counterpart and inhibit their formation of crystalline structure. Thus, the ordered structure indicated by absorption spectroscopy is at most nanocrystalline in structure in the film, and the detection is beyond the capability of our XRD system. Only indirect evidence for increased ordering can be seen from the increase in the roughness of the films (discussed in the following), increased inter-band absorption from absorption spectra and increased mobility from TOF measurements.

Figure 5 shows the atomic force microscopy (AFM) images of the slow-grown (no. 1) and fast-grown (no. 7) films, before and after thermal annealing. For film no. 1, the surface is very rough with r.m.s. roughness, σ, of 11.5 nm (Fig. 5a). The film

after 10 min of annealing at 110 °C shows similar $\sigma \sim 9.5$ nm (Fig. 5b), but the texture is smoother than that of un-annealed film. For film no. 7, a very smooth surface with $\sigma \sim 0.87$ nm is observed (Fig. 5c). After heating at 110 °C for 20 min, the roughness increases with $\sigma \sim 1.9$ nm (Fig. 5d). By comparing these results with device performance, we first suspected that the rough surface may effectively reduce the charge-transport distance and increase the J_{SC}, at the same time providing nanoscaled texture that further enhances internal light scattering and light absorption. However, using the surface-area calculation function in our AFM program, the surface area in the roughest film was found to be only 0.4% more than that of an absolutely flat film. Thus, these mechanisms can only account for minor efficiency improvement at most. Instead, the rough surface is probably a signature of polymer (blend) self-organization, which in turn enhances ordered structure formation in the thin film. This assumption is strongly supported by (i) the very rough surface of slow-grown thick film, (ii) significant roughness increment after annealing of fast-grown thick film and (iii) roughness increment after annealing of thin films[18], all of which significantly enhance device efficiency. The peak to valley height of the slow-grown film is ~100 nm, corresponding to ~50% of the mean thickness. Thermal annealing of P3AT films has been shown to enhance crystallization and increase the μ_h in PV cells[5]. However, this might not be true for well-ordered thick films such as those in our case, as seen from the absorption spectra and no significant increase in J_{SC} on annealing. We observed that FFs tended to increase when devices were left in the vacuum for long times. Thus, we suspect annealing the slow-grown films might mainly help in removing the residue solvent, reducing the free volume and improving the interface with the electrode, instead of inducing further self-organization in already ordered films. As a result of annealing, the number of trapping sites is reduced for carrier transport and extraction. Another possible mechanism is the improvement of cathode contact from morphology change. After annealing, the surface of slow-grown film becomes smoother and this in turn improves the organic/cathode contact. Annealing at 110 °C reduces R_{SA} from 2.41 to 1.56 Ω cm^2, which is among the lowest values reported for similar device dimensions. Along with a better balanced charge transport this gives a very high FF of 67.4% and the PCE of 4.4%. Similar series resistance values have been reported earlier for devices based on P3HT[11,27], poly(*p*-phenylenevinylene) derivative[28] and copper phthalocyanine[29]; however, in our case the carrier transport is more balanced, as observed from the TOF measurements.

These results will help in better understanding the underlying relationship between the polymer morphology and the device performance and will subsequently help in enhancing the efficiencies of plastic solar cells to a level of practical applications.

METHODS

The polymer PV devices were fabricated by spin-coating a blend of P3HT/PCBM in 1:1 wt/wt ratio, sandwiched between a transparent anode and a cathode. The anode consisted of glass substrates pre-coated with indium tin oxide (ITO), modified by spin-coating polyethylenedioxythiophene/polystyrenesulphonate (PEDOT/PSS) layer (~25 nm), and the cathode consisted of Ca (~25 nm) capped with Al (~80 nm). Before device fabrication, the ITO-coated (~150 nm) glass substrates were cleaned by ultrasonic treatment in detergent, deionized water, acetone and isopropyl alcohol sequentially. A thin layer (~30 nm) of PEDOT/PSS (Baytron P VP A1 4083) was spin-coated to modify the ITO surface. After baking at 120 °C for 1 h, the substrates were transferred to a nitrogen-filled glove box (<0.1 p.p.m. O_2 and H_2O). P3HT (purchased from Rieke Metals, used as received) was first dissolved in 1,2-dichlorobenzene (DCB) to make 17 mg ml^{-1} solution, followed by blending with PCBM (purchased from Nano-C, used as received) in 50 wt%. The blend was stirred for ~14 h at 40 °C in the glove box. The active layer was obtained by spin-coating the blend at 600 r.p.m. for 60 s and the thickness of film was ~210–230 nm, as measured with a Dektek profilometer. The active device area was 0.11 cm^2. Spin-coating at 600 r.p.m. left the films wet, which were then dried in covered glass petri dishes. Before cathode deposition, the films were thermally annealed at 110 °C for various times. Testing was done in N_2 under simulated AM1.5G irradiation (100 mW cm^{-2}) using a xenon-lamp-based solar simulator (Oriel 96000 150W Solar Simulator). The films used in TOF measurements were spun-cast on ITO-coated glass substrates from P3HT/PCBM 1:1 wt/wt ratio solution (100 mg ml^{-1} total, DCB as solvent) and then Al was deposited as electrode. Immediately following the spin-coating, the films were either kept in covered petri dish for slow growth or were baked at 70 °C for ~30 s for fast growth. The thickness of the films for TOF measurements was ~1 μm. The absorption spectra were taken using a Varian Cary 50 Ultraviolet–Visible Spectrophotometer. To mimic the device fabrication conditions, all of the films were spun-cast on PEDOT/PSS-covered silica glass, also used as the absorption baseline. A Digital Instruments Multimode Scanning Probe Microscope was used to obtain the AFM images. The film preparation conditions for the AFM measurements were kept the same as device fabrication for accurate comparison.

Encapsulated devices were brought to NREL, Colorado, for testing of PCE and EQE under STC. NREL measured a set of devices, the best yielding 3.6% efficiency. There was a mismatch between the results for the same devices as measured at UCLA, probably the result of spectral mismatch primarily owing to a poorly matched reference cell. Although the open circuit voltages and FFs were the same, the currents and efficiencies as measured by NREL were only 84% of those measured in our lab. This 0.84 correction factor was applied to the larger set of devices measured at UCLA to obtain correct efficiency values. The efficiency values reported in this work are all after the correction. Although the efficiency values are calibrated, we did not consider three important factors: (i) device degradation during shipping to NREL owing to non-ideal encapsulation; (ii) reduction in effective device area on reaction with epoxy after encapsulation; and (iii) the optical losses owing to reflection by glass substrate and absorption from ITO.

Received 11 March 2005; accepted 19 August 2005; published 9 October 2005.

References

1. Brabec, C. J., Sariciftci, N. S. & Hummelen, J. C. Plastic solar cells. *Adv. Funct. Mater.* **11,** 15–26 (2001).
2. Coakley, K. M. & McGehee, M. D. Conjugated polymer photovoltaic cells. *Chem. Mater.* **16,** 4533–4542 (2004).
3. Brabec, C. J. Organic photovoltaics: technology and market. *Solar Energy Mater. Solar Cells* **83,** 273–292 (2004).
4. Shaheen, S. E. *et al.* 2.5% efficient organic plastic solar cells. *Appl. Phys. Lett.* **78,** 841–843 (2001).
5. Padinger, F., Rittberger, R. S. & Sariciftci, N. S. Effects of post production treatment on plastic solar cells. *Adv. Funct. Mater.* **13,** 85–88 (2003).
6. Walduf, C., Schilinsky, P., Hauch, J. & Brabec, C. J. Material and device concepts for organic photovoltaics: towards competitive efficiencies. *Thin Solid Films* **451–452,** 503–507 (2004).
7. Yu, G., Gao, J., Hummelen, J. C., Wudl, F. & Heeger, A. J. Polymer photovoltaic cells: enhanced efficiencies via a network of internal donor-acceptor heterojunctions. *Science* **270,** 1789–1791 (1995).
8. Saraciftci, N. S., Smilowitz, L., Heeger, A. J. & Wudl, F. Photoinduced electron transfer from a conducting polymer to buckminsterfullerene. *Science* **258,** 1474–1476 (1992).
9. Peumans, P., Uchida, S. & Forrest, S. R. Efficient bulk-heterojunction photovoltaic cells using small-molecular-weight organic thin films. *Nature* **425,** 158–162 (2003).
10. Yang, F., Shtein, M. & Forrest, S. R. Controlled growth of a molecular bulk heterojunction photovoltaic cell. *Nature Mater.* **4,** 37–41 (2005).
11. Chirvase, D., Parisi, J., Hummelen, J. C. & Dyakonov, V. Influence of nanomorphology on the photovoltaic action of polymer-fullerene composites. *Nanotechnology* **15,** 1317–1323 (2004).
12. Shrotriya, V., Ouyang, J., Tseng, R. J., Li, G. & Yang, Y. Absorption spectra modification in poly(3-hexylthiophene):methanofullerene blend thin films. *Chem. Phys. Lett.* **411,** 138–143 (2005).
13. Grevin, B., Rannou, P., Payerne, R., Pron, A. & Travers, J. P. Multi-scale scanning tunneling microscopy imaging of self-organized regioregular poly(3-hexylthiophene) films. *J. Chem. Phys.* **118,** 7097–7102 (2003).
14. Sirringhaus, H. *et al.* Two-dimensional charge transport in self-organized, high-mobility conjugated polymers. *Nature* **401,** 685–688 (1999).
15. Bao, Z., Dodabalapur, A. & Lovinger, A. J. Soluble and processable regioregular poly(3-hexylthiophene) for thin film field-effect transistor applications with high mobility. *Appl. Phys. Lett.* **69,** 4108–4110 (1996).
16. Melzer, C., Koop, E. J., Mihailetchi, V. D. & Blom, P. W. M. Hole transport in poly(phenylene vinylene)/methanofullerene bulk-heterojunction solar cells. *Adv. Funct. Mater.* **14,** 865–870 (2004).
17. Shirland, F. The history, design, fabrication and performance of CdS thin film solar cells. *Adv. Energy Conversion* **6,** 201–222 (1966).
18. Li, G., Shrotriya, V., Yao, Y. & Yang, Y. Investigation of annealing effects and film thickness dependence of polymer solar cells based on poly(3-hexylthiophene). *J. Appl. Phys.* **98,** 043704 (2005).
19. Choulis, S. A. *et al.* Investigation of transport properties in polymer/fullerene blends using time-of-flight photocurrent measurements. *Appl. Phys. Lett.* **83,** 3812–3814 (2003).
20. Mihailetchi, V. D. *et al.* Compositional dependence of the performance of poly(p-phenylenevinylene):methanofullerene bulk-heterojunction solar cells. *Adv. Funct. Mater.* **15,** 795–801 (2005).
21. Goodman, A. M. & Rose, A. Double extraction of uniformly generated electron–hole pairs from insulators with noninjecting contacts. *J. Appl. Phys.* **42,** 2823–2830 (1971).
22. Snaith, H. L., Greenham, N. C. & Friend, R. H. The origin of collected charge and open-circuit voltage in blended polyfluorene photovoltaic devices. *Adv. Mater.* **16,** 1640–1645 (2004).
23. Sunderberg, M., Inganas, O., Stafstrom, S., Gustafsson, G. & Sjogren, B. Optical absorption of poly(3-alkylthiophenes) at low temperatures. *Solid State Commun.* **71,** 435–439 (1989).
24. Prosa, T. J., Moulton, J., Heeger, A. J. & Winokur, M. J. Diffraction line-shape analysis of poly(3-docecylthiophene): A study of layer disorder through the liquid crystalline polmer transition. *Macromolecules* **32,** 4000–4009 (1999).
25. Aasmundtveit, K. E. *et al.* Structural anisotropy of poly(alkylthiophene) films. *Macromolecules* **33,** 3120–3127 (2000).
26. Samuelsen, E. J., Breiby, D. W., Konovalov, O., Struth, B. & Smilgies, D. -M. In situ studies of transition from solution to solid film of poly(octylthiophene). *Synth. Met.* **123,** 165–170 (2001).
27. Schilinsky, P., Waldauf, C., Hauch, J. & Brabec, C. J. Simulation of light intensity dependent current characteristics of polymer solar cells. *J. Appl. Phys.* **95,** 2816–2819 (2004).
28. Mozer, A. J. *et al.* Novel regiospecific MDMO-PPV copolymer with improved charge transport for bulk heterojunction solar cells. *J. Phys. Chem. B* **108,** 5235–5242 (2004).
29. Xue, J., Uchida, S., Rand, B. P. & Forrest, S. R. 4.2% efficient organic photovoltaic cells with low series resistance. *Appl. Phys. Lett.* **84,** 3013–3015 (2004).

Acknowledgements

We thank J. Ouyang for very helpful technical discussions. This research work is supported in part by the Office of Naval Research (grant no. N00014-01-1-0136, program manager P. Armistead), and the Air Force Office of Scientific Research (grant no. F49620-03-1-0101, program manager C. Lee). Correspondence and requests for materials should be addressed to Y.Y.

Competing financial interests

The authors declare that they have no competing financial interests.